Accurate Model of Arbitrary Wire Antennas in Free Space, Above or Inside Ground

Tie Jun Cui, *Member, IEEE* and Weng Cho Chew, *Fellow, IEEE*

***Abstract*—An accurate model of wire antennas in free space, above or inside lossy ground is presented in which the current is assumed to flow on the surface of the wire and the testing is also performed on the surface. To replace the traditional delta-gap source, a more accurate source model is developed by using the Huygens' principle. From this principle and reciprocity theorem, a variational formulation of the input admittance is derived. When the triangle function is chosen as both basis and weighting functions, all the elements of impedance matrix and source vector are formulated in closed forms, which can be rapidly computed. Several numerical results are given. Comparing with measured data, both the current distribution and input impedance by this model are more accurate than those of delta-gap model.**

***Index Terms*—Accurate model, Galerkin method, Sommerfeld integrals, variational formula, wire antennas.**

I. Introduction

THE investigation of wire antennas in free space, above or inside lossy ground is a very old but important topic. For wires in free space, comprehensive study has been made by using approximate methods and numerical methods since the beginning of this century [1]–[13]. For wire antennas above or inside the lossy ground, they were intensively investigated in 1960's, 1970's, and early 1980's [14]–[23], after the pioneering work of Sommerfeld in 1909 [2]. In the above studies, the method of moments [7] plays an important role in modeling arbitrary wire antennas, yielding some efficient codes, for example, the numerical electromagnetics code (NEC) [21], [22]. Recently, we developed a general algorithm for wire antennas above or inside the lossy ground by using Galerkin's method with triangle basis function [26].

In the above methods, however, there are three limitations. First, in most methods the current is assumed to flow on the axis of the wire and testing is performed on the surface or vice versa. Second, the delta gap and magnetic frill are adopted for the source model but the delta gap is popularly used. In the frill model, a circumferentially directed magnetic current density that exists over an annular aperture with inner radius a and outer radius b has been assumed, requiring an additional parameter b [13]. Finally, the input admittance of the wire is simply defined as the ratio of the current and voltage at the driving point which is not variational.

Manuscript received February 5, 1999; revised January 6, 2000. This work was supported by DOE DEFG07-97ER 14835, AFOSR under MURI Grant F49620-96-1-0025, ONR under Grant N00014-95-1-0872, and Grant NSF ECS93-02145.

The authors are with the Center for Computational Electromagnetics, Department of Electrical and Computer Engineering, University of Illinois at Urbana-Champaign, Urbana, IL 61801-2991 USA.

Publisher Item Identifier S 0018-926X(00)03253-1.

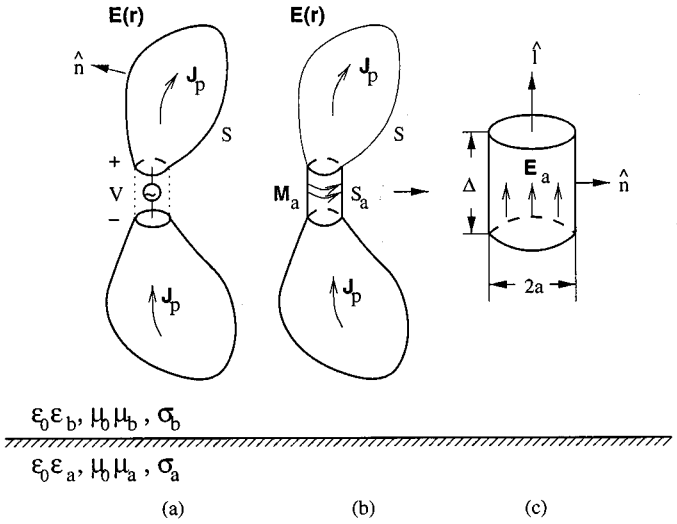

Fig. 1. A voltage-driven antenna and its equivalence. (a) Original problem. (b) Equivalent problem. (c) The source model.

In this paper, an accurate model of wire antennas in free space, above or inside lossy ground is presented in which the current is assumed to flow on the surface of the wire and the testing is also performed on the surface. To replace the delta-gap source, a more accurate source model is developed using Huygens' principle. From this principle and the reciprocity theorem, a variational formulation of the input admittance is derived in a general form. When the Galerkin's method with triangle basis function is used, all the elements of the impedance matrix and source vector are formulated in closed forms, which can be rapidly computed.

II. General Formulation

We consider a general three-dimensional (3-D) antenna in a half-space shown in Fig. 1(a). When $\epsilon_b = \epsilon_a = \mu_a = \mu_b = 1$ and $\sigma_a = \sigma_b = 0$, the antenna is in free space; when $\epsilon_b = \mu_b = 1$ and $\sigma_b = 0$, the antenna is above the ground; when $\epsilon_a = \mu_a = 1$ and $\sigma_a = 0$, the antenna is inside the ground. From Huygens' principle, the electric field $\boldsymbol{E}(\boldsymbol{r})$ can be expressed as

$$\boldsymbol{E}(\boldsymbol{r}) = -\nabla \times \oint_S dS' \overline{\boldsymbol{G}}_m(\boldsymbol{r}, \boldsymbol{r}') \cdot \hat{n}' \times \boldsymbol{E}(\boldsymbol{r}') + i\omega\mu_0\mu_b \oint_S dS' \overline{\boldsymbol{G}}_e(\boldsymbol{r}, \boldsymbol{r}') \cdot \hat{n}' \times \boldsymbol{H}(\boldsymbol{r}') \quad (1)$$

in which $\boldsymbol{H}(\boldsymbol{r}')$ is the magnetic field and $\overline{\boldsymbol{G}}_e(\boldsymbol{r}, \boldsymbol{r}')$ and $\overline{\boldsymbol{G}}_m(\boldsymbol{r}, \boldsymbol{r}')$ are electric- and magnetic-field dyadic Green's functions. From the reciprocity theorem $\langle \boldsymbol{M}_2, \boldsymbol{H}_1 \rangle = -\langle \boldsymbol{J}_1, \boldsymbol{E}_2 \rangle$,

it is easily shown that $\overline{G}_m(\boldsymbol{r}, \boldsymbol{r}')$ has a relation with $\overline{G}_e(\boldsymbol{r}, \boldsymbol{r}')$ [27]

$$\nabla \times \overline{G}_m(\boldsymbol{r}, \boldsymbol{r}') = \left[\nabla' \times \overline{G}_e(\boldsymbol{r}', \boldsymbol{r})\right]^t \tag{2}$$

where "t" represents the transpose. In the half-space problem shown in Fig. 1, the dyadic Green's function $\overline{G}_e(\boldsymbol{r}, \boldsymbol{r}')$ is expressed as [25], [26]

$$\begin{aligned}\hat{\alpha} \cdot \overline{G}_e \cdot \hat{\alpha}' &= \frac{i\omega\mu_0\mu_b}{4\pi}\left(\hat{\alpha}\cdot\hat{\alpha}' + \frac{1}{k_b^2}\,\hat{\alpha}\cdot\nabla\nabla\cdot\hat{\alpha}'\right) g^P \\ &\quad + \frac{i\omega\mu_0\mu_b}{4\pi}\left(\vec{\alpha}_s\cdot\vec{\alpha}_s' g^R_{\mathrm{TE}} + \alpha_z\alpha_z' g^R_{\mathrm{TM}}\right) \\ &\quad + \frac{i\omega\mu_0\mu_b}{4\pi k_b^2}\left(\hat{\alpha}\cdot\nabla\nabla\cdot\hat{\alpha}'' g^R_{\mathrm{TM}} + 2\vec{\alpha}_s\cdot\nabla_s\nabla_s\cdot\vec{\alpha}_s' g^R_{\mathrm{EM}}\right)\end{aligned} \tag{3}$$

where

$$g^P(\boldsymbol{r}-\boldsymbol{r}') = \frac{\exp(ik_b|\boldsymbol{r}-\boldsymbol{r}'|)}{|\boldsymbol{r}-\boldsymbol{r}'|} \tag{4}$$

$$\begin{aligned}&g^R_{\mathrm{TE,\,TM,\,EM}}(\boldsymbol{r}_s - \boldsymbol{r}_s', z+z') \\ &\quad = \frac{i}{2\pi}\int_{-\infty}^{+\infty}\int_{-\infty}^{+\infty}\frac{R^{\mathrm{TE,\,TM,\,EM}}}{k_{bz}} \\ &\qquad \cdot e^{i\boldsymbol{k}_s\cdot(\boldsymbol{r}_s-\boldsymbol{r}_s')+ik_{bz}(z+z')}\,d\boldsymbol{k}_s\end{aligned} \tag{5}$$

in which R^{TE} and R^{TM} are reflection coefficients of TE wave and TM wave in Region b, and R^{EM} is a mixed reflection coefficient, which are defined by

$$R^{\mathrm{TE}} = \frac{\mu_a k_{bz} - \mu_b k_{az}}{\mu_a k_{bz} + \mu_b k_{az}}, \qquad R^{\mathrm{TM}} = \frac{\tilde{\epsilon}_a k_{bz} - \tilde{\epsilon}_b k_{az}}{\tilde{\epsilon}_a k_{bz} + \tilde{\epsilon}_b k_{az}},$$
$$R^{\mathrm{EM}} = \frac{k_b^2}{2k_s^2}\left(R^{\mathrm{TM}} + R^{\mathrm{TE}}\right).$$

In above expressions, $\hat{\alpha} = \vec{\alpha}_s + \hat{z}\alpha_z$ is a unit vector denoting the direction of electric field at the observation point; $\hat{\alpha}' = \vec{\alpha}_s' + \hat{z}\alpha_z'$ is that for the source point; $\hat{\alpha}'' = -\vec{\alpha}_s' + \hat{z}\alpha_z'$ is that for an image source point; $\boldsymbol{r} = \boldsymbol{r}_s + \hat{z}z$; $\nabla = \nabla_s + \hat{z}\partial/\partial z$ in which the subscript "s" represents the transverse direction: $\boldsymbol{r}_s = \hat{x}x + \hat{y}y$, $\nabla_s = \hat{x}\partial/\partial x + \hat{y}\partial/\partial y$, $\boldsymbol{k}_s = \hat{x}k_x + \hat{y}k_y$, $k_s^2 = k_x^2 + k_y^2$. Furthermore, $k_{jz} = \sqrt{k_j^2 - k_s^2}$ where $k_j = k_0\sqrt{\mu_j\tilde{\epsilon}_j}$ is the wave number in Region j ($\tilde{\epsilon}_j = \epsilon_j + i\sigma_j/\omega\epsilon_0$) and k_0 is the wave number in the free space.

In (1), $\hat{n}' \times \boldsymbol{E}(\boldsymbol{r}')$ equals zero on S except on S_a. Thus, the original problem in Fig. 1(a) is equivalent to (b) where S is a closed metallic surface, and an equivalent magnetic current $\boldsymbol{M}_a$ is impressed on the part of the metallic surface where originally in Fig. 1(a), it was a gap. Then the field $\boldsymbol{E}(\boldsymbol{r})$ can be written as

$$\begin{aligned}\boldsymbol{E}(\boldsymbol{r}) = &\nabla \times \oint_{S_a} dS'\overline{G}_m(\boldsymbol{r}, \boldsymbol{r}')\cdot\boldsymbol{M}_a(\boldsymbol{r}') \\ &+ i\omega\mu_0\mu_b \oint_S dS'\overline{G}_e(\boldsymbol{r}, \boldsymbol{r}')\cdot\boldsymbol{J}_p(\boldsymbol{r}')\end{aligned} \tag{6}$$

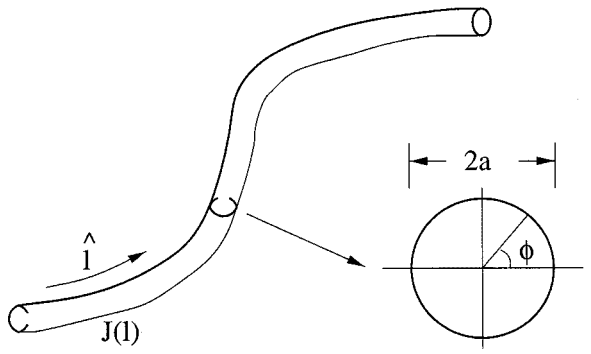

Fig. 2. An arbitrary wire antenna and its cross section.

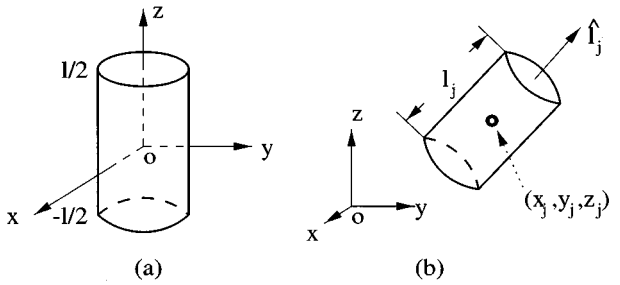

Fig. 3. A segment of the wire antenna: (a) local coordinate and (b) global coordinate.

in which S_a is the aperture region of the surface and $S_a \in S$; $\boldsymbol{M}_a = -\hat{n}\times\boldsymbol{E}_a$ is assumed known and $\boldsymbol{J}_p$ is the induced current on the closed metallic surface S which has to be solved for.

When the gap Δ is small and driving voltage is V, the magnetic current density can be expressed as

$$\boldsymbol{M}_a = -\hat{n}\times\boldsymbol{E}_a = -\hat{n}\times\hat{l}\frac{V}{\Delta} \tag{7}$$

as shown in Fig. 1(c).

Using the boundary condition on the metallic surface S, one obtains the integral equation for the induced electric current density

$$\begin{aligned}&i\omega\mu_0\mu_b \oint_S dS'\overline{G}_e(\boldsymbol{r}, \boldsymbol{r}')\cdot\boldsymbol{J}_p(\boldsymbol{r}') \\ &\quad = -\nabla\times\oint_{S_a} dS'\overline{G}_m(\boldsymbol{r}, \boldsymbol{r}')\cdot\boldsymbol{M}_a(\boldsymbol{r}'), \quad \boldsymbol{r}\in S\end{aligned} \tag{8}$$

which can be solved by the method of moments. Choosing the basis function and letting

$$\boldsymbol{J}_p(\boldsymbol{r}') = \sum_{n=1}^{N} I_n\boldsymbol{J}_n(\boldsymbol{r}') \tag{9}$$

then testing with $\boldsymbol{w}_m(\boldsymbol{r})$ yields

$$\overline{\boldsymbol{Z}}\cdot\boldsymbol{I} = \boldsymbol{V} \tag{10}$$

in which the impedance matrix $\overline{\boldsymbol{Z}}$ and source vector (or voltage vector) $\boldsymbol{V}$ are given by

$$Z_{mn} = i\omega\mu_0\mu_b\langle\boldsymbol{w}_m(\boldsymbol{r}), \overline{G}_e(\boldsymbol{r}, \boldsymbol{r}'), \boldsymbol{J}_n(\boldsymbol{r}')\rangle \tag{11}$$

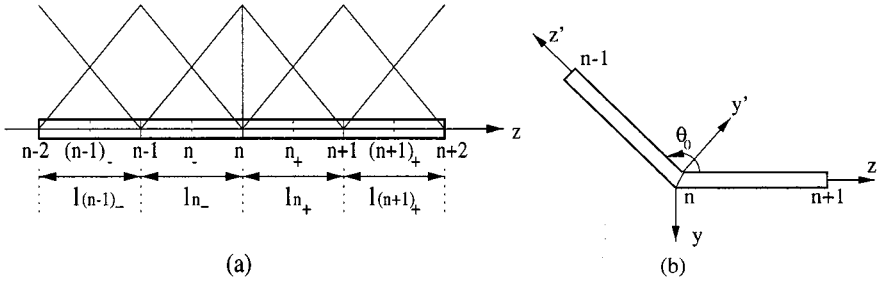

Fig. 4. Adjacent nodes of the wire antenna. (a) Nonjunction node. (b) Junction node.

TABLE I
PARAMETERS OF ADJACENT NODES

(i,j)	z_1	z_2	t_1	t_2	u_1	u_2	v_1	v_2
n_-, n_-	$-l_{n_-}$	0	$-l_{n_-}$	0	1	$l_{n_-}^{-1}$	1	$l_{n_-}^{-1}$
$n_-, (n-1)_+$	$-l_{n_-}$	0	$-l_{n_-}$	0	1	$l_{n_-}^{-1}$	0	$-l_{n_-}^{-1}$
$n_-, (n-1)_-$	$-l_{n_-}$	0	$-l_{n_-} - l_{(n-1)_-}$	$-l_{n_-}$	1	$l_{n_-}^{-1}$	$1 + l_{(n-1)_-}^{-1} l_{n_-}$	$l_{(n-1)_-}^{-1}$
$n_-, (n-2)_+$	$-l_{n_-}$	0	$-l_{n_-} - l_{(n-1)_-}$	$-l_{n_-}$	1	$l_{n_-}^{-1}$	$-l_{(n-1)_-}^{-1} l_{n_-}$	$-l_{(n-1)_-}^{-1}$
n_-, n_+	$-l_{n_-}$	0	0	l_{n_+}	1	$l_{n_-}^{-1}$	1	$-l_{n_+}^{-1}$
$n_-, (n+1)_-$	$-l_{n_-}$	0	0	l_{n_+}	1	$l_{n_-}^{-1}$	0	$l_{n_+}^{-1}$
n_+, n_+	0	l_{n_+}	0	l_{n_+}	1	$-l_{n_+}^{-1}$	1	$-l_{n_+}^{-1}$
$n_+, (n+1)_-$	0	l_{n_+}	0	l_{n_+}	1	$-l_{n_+}^{-1}$	0	$l_{n_+}^{-1}$
$n_+, (n+1)_+$	0	l_{n_+}	l_{n_+}	$l_{n_+} + l_{(n+1)_+}$	1	$-l_{n_+}^{-1}$	$1 + l_{(n+1)_+}^{-1} l_{n_+}$	$-l_{(n+1)_+}^{-1}$
$n_+, (n+2)_-$	0	l_{n_+}	l_{n_+}	$l_{n_+} + l_{(n+1)_+}$	1	$-l_{n_+}^{-1}$	$-l_{(n+1)_+}^{-1} l_{n_+}$	$l_{(n+1)_+}^{-1}$
n_+, n_-	0	l_{n_+}	$-l_{n_-}$	0	1	$-l_{n_+}^{-1}$	1	$l_{n_-}^{-1}$
$n_+, (n-1)_+$	0	l_{n_+}	$-l_{n_-}$	0	1	$-l_{n_+}^{-1}$	0	$-l_{n_-}^{-1}$

and

$$V_m = -\langle \boldsymbol{w}_m(\boldsymbol{r}), \nabla \times \overline{\boldsymbol{G}}_m(\boldsymbol{r}, \boldsymbol{r}'), \boldsymbol{M}_a(\boldsymbol{r}') \rangle \tag{12}$$

and $\boldsymbol{J}_n(\boldsymbol{r}')$ and $\boldsymbol{w}_m(\boldsymbol{r})$ are basis and testing or weighting functions, respectively.

After $\boldsymbol{J}_p(\boldsymbol{r}')$ is solved for, a variational expression for the general input admittance is [28]

$$Y_{\text{in}} = -\frac{\langle \boldsymbol{M}_a, \boldsymbol{H}_T \rangle}{V^2} + \frac{\langle \boldsymbol{E}_T, \boldsymbol{J}_p \rangle}{V^2} \tag{13}$$

where

$\boldsymbol{E}_T$ and $\boldsymbol{H}_T$ are the total electric and magnetic fields produced by both $\boldsymbol{M}_a$ and $\boldsymbol{J}_p$;
$\langle \boldsymbol{M}_a, \boldsymbol{H}_T \rangle$ is defined on S_a, while
$\langle \boldsymbol{E}_T, \boldsymbol{J}_p \rangle$ is defined on S.

For the exact solution, $\langle \boldsymbol{E}_{Te}, \boldsymbol{J}_p \rangle = 0$ since the tangential electric field equals zero on the metallic surface. Then

$$Y_{\text{in}} = -\frac{\langle \boldsymbol{M}_a, \boldsymbol{H}_{Te} \rangle}{V^2} \tag{14}$$

where $\boldsymbol{E}_{Te}$ and $\boldsymbol{H}_{Te}$ are the exact total fields. We take the first-order variation of (13) about the exact solution to show that

$$\delta Y_{\text{in}} = -\frac{\langle \boldsymbol{M}_a, \delta \boldsymbol{H} \rangle}{V^2} + \frac{\langle \delta \boldsymbol{E}, \boldsymbol{J}_{pe} \rangle}{V^2} + \frac{\langle \boldsymbol{E}_{Te}, \delta \boldsymbol{J} \rangle}{V^2} \tag{15}$$

in which we assume that $\boldsymbol{J}_p = \boldsymbol{J}_{pe} + \delta \boldsymbol{J}$ but $\boldsymbol{M}_a$ remains unchanged since the antenna in Fig. 1(a) is driven by a voltage source. Due to the fact that the tangential electric field on S equals zero, the last term in (15) is obviously zero.

From the reciprocity theorem, we have $\langle \boldsymbol{E}_a, \boldsymbol{J}_{pe} \rangle = -\langle \boldsymbol{H}_{pe}, \boldsymbol{M}_a \rangle$. Since $\boldsymbol{M}_a$ and $\boldsymbol{E}_a$ are unchanged, one obtains

$$\langle \boldsymbol{E}_a, \delta \boldsymbol{J} \rangle = -\langle \delta \boldsymbol{H}, \boldsymbol{M}_a \rangle = -\langle \boldsymbol{M}_a, \delta \boldsymbol{H} \rangle.$$

Considering $\hat{t} \cdot \boldsymbol{E}_{Te} = \hat{t} \cdot (\boldsymbol{E}_{pe} + \boldsymbol{E}_a) = 0$ on S, where $\hat{t}$ is a unit tangential vector on S, the above equation gives

$$\langle \boldsymbol{M}_a, \delta \boldsymbol{H} \rangle = \langle \boldsymbol{E}_{pe}, \delta \boldsymbol{J} \rangle. \tag{16}$$

Similarly, using the reciprocity theorem, we have

$$\langle \boldsymbol{E}_{pe}, \delta \boldsymbol{J} \rangle = \langle \delta \boldsymbol{E}, \boldsymbol{J}_{pe} \rangle. \tag{17}$$

Substituting (16) and (17) into (15) yields $\delta Y_{\text{in}} = 0$, which implies that (13) is a variational formula about the exact solution.

If Galerkin's method is used, then $\boldsymbol{w}_m(\boldsymbol{r}) = \boldsymbol{J}_m(\boldsymbol{r})$ and it is easily shown that $\langle \boldsymbol{E}_T, \boldsymbol{J}_p \rangle = 0$ even for approximate $\boldsymbol{E}_T$ and $\boldsymbol{J}_p$. In this case, only the first term in (13) remains or

$$Y_{\text{in}} = -\frac{\langle \boldsymbol{M}_a, \boldsymbol{H}_T \rangle}{V^2}. \tag{18}$$

From the equivalent problem shown in Fig. 1(b), we easily have

$$\boldsymbol{H}(\boldsymbol{r}) = \nabla \times \oint_S dS' \overline{\boldsymbol{G}}_e(\boldsymbol{r}, \boldsymbol{r}') \cdot \boldsymbol{J}_p(\boldsymbol{r}') + i\omega\epsilon_0 \tilde{\epsilon}_b \oint_{S_a} dS' \overline{\boldsymbol{G}}_m(\boldsymbol{r}, \boldsymbol{r}') \cdot \boldsymbol{M}_a(\boldsymbol{r}') \quad \boldsymbol{r} \in S_a. \tag{19}$$

TABLE II
PART OF THE IMPEDANCE MATRIX Z_{mn} OF A HALF-WAVELENGTH DIPOLE IN THE FREE-SPACE ($L = 0.5$ m, $N = 21$, $f = 300$ MHz)

$a = 0.2$ mm

m	n	This model	The old model
11	1	(0.330, 0.662)	(0.330, 0.662)
11	2	(0.344, 0.887)	(0.344, 0.887)
11	3	(0.357, 1.217)	(0.357, 1.217)
11	4	(0.368, 1.737)	(0.368, 1.737)
11	5	(0.378, 2.627)	(0.378, 2.627)
11	6	(0.387, 4.417)	(0.387, 4.417)
11	7	(0.394, 8.518)	(0.394, 8.518)
11	8	(0.400, 21.526)	(0.400, 21.526)
11	9	(0.396, 143.102)	(0.396, 143.598)
11	10	(0.380, 1406.263)	(0.380, 1404.523)
11	11	(0.401,-3125.479)	(0.401,-3122.986)

$a = 5$ mm

m	n	This model	The old model
11	1	(0.330, 0.661)	(0.330, 0.660)
11	2	(0.344, 0.884)	(0.344, 0.882)
11	3	(0.357, 1.212)	(0.357, 1.221)
11	4	(0.368, 1.727)	(0.368, 1.745)
11	5	(0.378, 2.607)	(0.378, 2.645)
11	6	(0.387, 4.365)	(0.387, 4.394)
11	7	(0.394, 8.346)	(0.394, 8.444)
11	8	(0.400, 20.568)	(0.400, 21.149)
11	9	(0.396, 96.741)	(0.404, 104.061)
11	10	(0.380, 248.372)	(0.407, 211.185)
11	11	(0.401, -742.167)	(0.408, -684.008)

$a = 15$ mm

m	n	This model	The old model
11	1	(0.329, 0.646)	(0.329, 0.653)
11	2	(0.343, 0.861)	(0.343, 0.871)
11	3	(0.355, 1.174)	(0.356, 1.201)
11	4	(0.367, 1.656)	(0.368, 1.707)
11	5	(0.377, 2.459)	(0.378, 2.566)
11	6	(0.386, 3.988)	(0.386, 4.192)
11	7	(0.393, 7.173)	(0.394, 7.786)
11	8	(0.399, 15.293)	(0.399, 17.695)
11	9	(0.394, 46.841)	(0.403, 50.114)
11	10	(0.378, 71.934)	(0.406, 15.723)
11	11	(0.399, -284.438)	(0.407, -185.780)

Then $\boldsymbol{H}_T$ in (18) should be

$$\boldsymbol{H}_T(\boldsymbol{r}) = i\omega\epsilon_0\tilde{\epsilon}_b \oint_{S_a} dS'\overline{\boldsymbol{G}}_m(\boldsymbol{r},\boldsymbol{r}')\cdot\boldsymbol{M}_a(\boldsymbol{r}') + \nabla \times \sum_{n=1}^{N} I_n \oint_S dS'\overline{\boldsymbol{G}}_e(\boldsymbol{r},\boldsymbol{r}')\cdot\boldsymbol{J}_n(\boldsymbol{r}') \quad \boldsymbol{r}\in S_a. \tag{20}$$

Hence,

$$\langle \boldsymbol{M}_a, \boldsymbol{H}_T\rangle = i\omega\epsilon_0\tilde{\epsilon}_b\langle \boldsymbol{M}_a(\boldsymbol{r}), \overline{\boldsymbol{G}}_m(\boldsymbol{r},\boldsymbol{r}'), \boldsymbol{M}_a(\boldsymbol{r}')\rangle + \sum_{n=1}^{N} I_n\langle \boldsymbol{M}_a(\boldsymbol{r}), \nabla\times\overline{\boldsymbol{G}}_e(\boldsymbol{r},\boldsymbol{r}'), \boldsymbol{J}_n(\boldsymbol{r}')\rangle.$$

Thus,

$$Y_{\text{in}} = -i\omega C^a_{\text{in}} + Y^p_{\text{in}} \tag{21}$$

in which C^a_{in} and Y^p_{in} are the gap capacitance and input admittance of the antenna

$$C^a_{\text{in}} = \frac{\epsilon_0\tilde{\epsilon}_b}{V^2}\langle \boldsymbol{M}_a(\boldsymbol{r}), \overline{\boldsymbol{G}}_m(\boldsymbol{r},\boldsymbol{r}'), \boldsymbol{M}_a(\boldsymbol{r}')\rangle, \tag{22}$$

$$Y^p_{\text{in}} = -\frac{1}{V^2}\sum_{n=1}^{N} I_n\langle \boldsymbol{M}_a(\boldsymbol{r}), \nabla\times\overline{\boldsymbol{G}}_e(\boldsymbol{r},\boldsymbol{r}'), \boldsymbol{J}_n(\boldsymbol{r}')\rangle. \tag{23}$$

Using relation (2),

$$\begin{aligned}\langle \boldsymbol{M}_a(\boldsymbol{r}), \nabla\times\overline{\boldsymbol{G}}_e(\boldsymbol{r},\boldsymbol{r}'), \boldsymbol{J}_n(\boldsymbol{r}')\rangle &= \langle \boldsymbol{J}_n(\boldsymbol{r}'), \left[\nabla\times\overline{\boldsymbol{G}}_e(\boldsymbol{r},\boldsymbol{r}')\right]^{\text{t}}, \boldsymbol{M}_a(\boldsymbol{r})\rangle \\ &= \langle \boldsymbol{J}_n(\boldsymbol{r}'), \nabla'\times\overline{\boldsymbol{G}}_m(\boldsymbol{r}',\boldsymbol{r}), \boldsymbol{M}_a(\boldsymbol{r})\rangle \\ &= \langle \boldsymbol{J}_n(\boldsymbol{r}), \nabla\times\overline{\boldsymbol{G}}_m(\boldsymbol{r},\boldsymbol{r}'), \boldsymbol{M}_a(\boldsymbol{r}')\rangle\end{aligned}$$

which is the same as (12) if Galerkin's method is used. Hence, the input admittance can finally be written as

$$Y^p_{\text{in}} = -\frac{1}{V^2}\sum_{n=1}^{N} I_n\langle \boldsymbol{J}_n(\boldsymbol{r}), \nabla\times\overline{\boldsymbol{G}}_m(\boldsymbol{r},\boldsymbol{r}'), \boldsymbol{M}_a(\boldsymbol{r}')\rangle. \tag{24}$$

Equation (24) is a general formula. The traditional definition of the input admittance is only a special case of this formula when the source vector (12) is a delta function.

III. WIRE ANTENNAS

For the wire antennas considered in this paper (see Fig. 2), we make the following assumptions.

- The current flows along the surface of the wire.
- The testing points are on the surface of the wire.
- The current is not a function of ϕ.
- The current is flowing in the longitudinal direction of the wire $\hat{l}$.
- The gap Δ and radius of the wire a are electrically small.

Under the above assumptions, the dyadic Green's function $\overline{\boldsymbol{G}}_e$ can be simplified by using directional derivative [26]. Then the impedance matrix is expressed as

$$Z_{mn} = Z^{(a)}_{mn}+Z^{(b)}_{mn}+Z^{(c)}_{mn}+Z^{(d)}_{mn}+Z^{(e)}_{mn}+Z^{(f)}_{mn}+Z^{(g)}_{mn}+Z^{(h)}_{mn}$$

where

$$Z^{(a)}_{mn} = -\frac{ik_0\eta_0\mu_b}{16\pi^3}\int_{\Delta S_m}\int_{\Delta S_n}\hat{l}_m\cdot\hat{l}'_n\, g^P(\boldsymbol{r}-\boldsymbol{r}')\cdot f_m(l)f_n(l')dS'dS \tag{25a}$$

$$Z^{(b)}_{mn} = \frac{ik_0\eta_0\mu_b}{16\pi^3 k_b^2}\int_{\Delta S_m}\int_{\Delta S_n} g^P(\boldsymbol{r}-\boldsymbol{r}')\cdot\frac{df_m(l)}{dl}\frac{df_n(l')}{dl'}\,dS'\,dS \tag{25b}$$

$$Z^{(c)}_{mn} = -\frac{ik_0\eta_0\mu_b}{16\pi^3 k_b^2}\int_{\Delta S_m}\int_{\Delta S_n} g^R_{\text{TM}}(\boldsymbol{r},\boldsymbol{r}')\cdot\frac{df_m(l)}{dl}\frac{df_n(l')}{dl'}\,dS'\,dS \tag{25c}$$

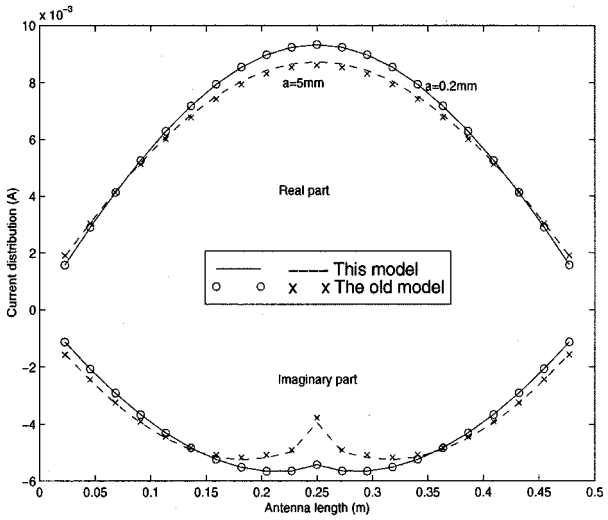

(a)

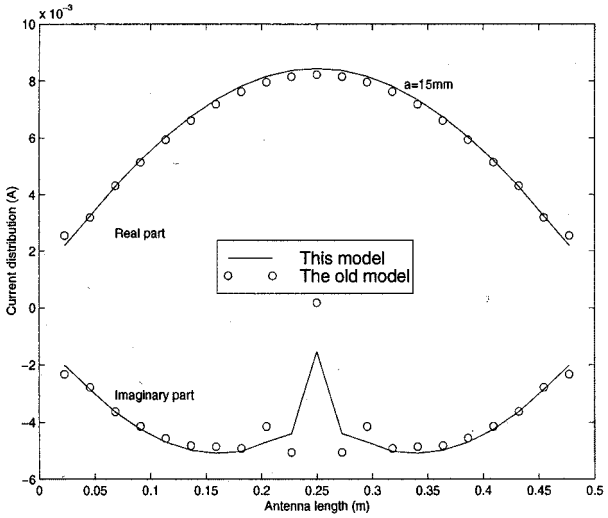

(b)

Fig. 5. Current distribution of a half-wavelength dipole with delta-gap source model: (a) $a = 0.2$ mm and $a = 5$ mm and (b) $a = 15$ mm.

$$Z_{mn}^{(d)} = \frac{ik_0\eta_0\mu_b}{8\pi^3 k_b^2} \int_{\Delta S_m}\int_{\Delta S_n} g_{\mathrm{EM}}^R(\boldsymbol{r},\boldsymbol{r}') \cdot \frac{df_m(l)}{dl}\,\frac{df_n(l')}{dl'}\,dS'\,dS \tag{25d}$$

$$Z_{mn}^{(e)} = \frac{ik_0\eta_0\mu_b}{8\pi^3 k_b^2} \int_{\Delta S_m}\int_{\Delta S_n} g_{\mathrm{EM1}}^R(\boldsymbol{r},\boldsymbol{r}') \cdot \alpha'_{zn}\,\frac{df_m(l)}{dl} f_n(l')\,dS'\,dS \tag{25e}$$

$$Z_{mn}^{(f)} = \frac{ik_0\eta_0\mu_b}{8\pi^3 k_b^2} \int_{\Delta S_m}\int_{\Delta S_n} g_{\mathrm{EM1}}^R(\boldsymbol{r},\boldsymbol{r}') \cdot \alpha_{zm}\,\frac{df_n(l')}{dl'} f_m(l)\,dS'\,dS \tag{25f}$$

$$Z_{mn}^{(g)} = \frac{ik_0\eta_0\mu_b}{8\pi^3 k_b^2} \int_{\Delta S_m}\int_{\Delta S_n} g_{\mathrm{EM2}}^R(\boldsymbol{r},\boldsymbol{r}') \cdot \alpha_{zm}\alpha'_{zn} f_m(l) f_n(l')\,dS'\,dS. \tag{25g}$$

$$Z_{mn}^{(h)} = -\frac{ik_0\eta_0\mu_b}{16\pi^3} \int_{\Delta S_m}\int_{\Delta S_n} \cdot \left[\vec{\alpha}_{sm}\cdot\vec{\alpha}'_{sn} g_{\mathrm{TE}}^R(\boldsymbol{r},\boldsymbol{r}') + \alpha_{zm}\alpha'_{zn} g_{\mathrm{TM}}^R(\boldsymbol{r},\boldsymbol{r}')\right] \cdot f_m(l) f_n(l')\,dS'\,dS \tag{25h}$$

in which $dS = dl\,d\phi$, $dS' = dl'\,d\phi'$, $\boldsymbol{r} = \boldsymbol{r}(l,\phi)$, $\boldsymbol{r}' = \boldsymbol{r}(l',\phi')$, $g_{\mathrm{EM1}}^R = (\partial/\partial z) g_{\mathrm{EM}}^R$, and $g_{\mathrm{EM2}}^R = (\partial^2/\partial z^2) g_{\mathrm{EM}}^R$. In (25a) and (25b) are the contributions from primary field, and (25c)–(25h) are the contributions from reflected field of the half space. In the reflected-field terms, the integrands are defined on the image region of ΔS_n. Therefore, when the antenna is not very close to the interface, the integral $\int d\phi \int d\phi'$ in these terms can be approximated by $4\pi^2$.

If we choose triangle function as the basis function, we will obtain the same expressions for $Z_{mn}^{(a)}$ to $Z_{mn}^{(h)}$ as those in [26] after improving the primary-field terms.

A. Impedance Matrix

The functions $\phi^P(i,j)$ and $\psi^P(i,j)$ in the primary-field terms [26] are defined as

$$\phi^P(i,j) = \frac{1}{4\pi^2}\int_{\Delta S_i}\int_{\Delta S_j} g^P(\boldsymbol{r}-\boldsymbol{r}') \cdot f_i(l) f_j(l')\,d\phi'\,d\phi\,dl'\,dl \tag{26a}$$

$$\psi^P(i,j) = \frac{1}{4\pi^2}\int_{\Delta S_i}\int_{\Delta S_j} g^P(\boldsymbol{r}-\boldsymbol{r}')\,d\phi'\,d\phi\,dl'\,dl \tag{26b}$$

which can be combined into a general form

$$h(i,j) = \frac{1}{4\pi^2}\int_{\Delta S_i}\int_{\Delta S_j} (u_1+u_2 l)(v_1+v_2 l') \cdot g^P(\boldsymbol{r}-\boldsymbol{r}')\,d\phi'\,d\phi\,dl'\,dl \tag{27}$$

with different parameters u_1, u_2, v_1 and v_2.

1) Mutual Term: We set up a local coordinate system as shown in Fig. 3(a) and evaluate the following integral:

$$K(x,y,z) = \frac{1}{2\pi}\int_{-l/2}^{l/2}(v_1+v_2 z')\int_0^{2\pi}\frac{e^{ik_b R}}{R}\,d\phi'\,dz' \tag{28}$$

in which $R^2 = \rho^2 + (z-z')^2 + a^2 - 2a\rho\cos(\phi-\phi')$. Since a is electrically small, we expand the integrand in terms of a by Taylor's series

$$p_1(a) = \frac{e^{ik_b R}}{R} \approx p_1(0) + a p_1'(0) + a^2\frac{p_1''(0)}{2} + O(a^3), \quad a \ll r_0$$

TABLE III
PART OF THE VOLTAGE VECTOR OF A HALF-WAVELEGNTH DIPOLE IN THE FREE-SPACE ($L = 0.5$ m, $\Delta = 22.7$ mm, $N = 21$, $f = 300$ MHz)

m	$a = 0.2$ mm	$a = 5$ mm	$a = 15$ mm
1	(.0000, 0.00000)	(.0001, -.00004)	(.0007, -.00034)
2	(.0000, 0.00000)	(.0001, -.00004)	(.0009, -.00036)
3	(.0000, 0.00000)	(.0001, -.00004)	(.0012, -.00037)
4	(.0000, 0.00000)	(.0002, -.00004)	(.0018, -.00038)
5	(.0000, 0.00000)	(.0003, -.00004)	(.0027, -.00039)
6	(.0000, 0.00000)	(.0005, -.00004)	(.0043, -.00040)
7	(.0000, 0.00000)	(.0010, -.00005)	(.0080, -.00041)
8	(.0000, 0.00000)	(.0024, -.00005)	(.0181, -.00041)
9	(.0000, 0.00000)	(.0091, -.00005)	(.0471, -.00042)
10	(.1253, 0.00000)	(.1636, -.00005)	(.1978, -.00042)
11	(.7494, 0.00000)	(.6488, -.00005)	(.4599, -.00042)

from which we obtain the inner integral of (28)

$$p_2(z') \approx \frac{e^{ik_b r_0}}{r_0}\left\{1+\frac{a^2}{2r_0^2}\left[(ik_b r_0-1) + \frac{\rho^2}{2r_0^2}(3-i3k_b r_0-k_b^2 r_0^2)\right]\right\}+O(a^3), \quad a \ll r_0$$

in which $r_0^2 = \rho^2 + (z-z')^2$. Similarly, expanding the function $p_2(z')$ in terms of z' by Taylor's series yields

$$\begin{aligned} K(x,y,z) &\approx v_1 l \frac{e^{ik_b r}}{r}\left\{1-\frac{a^2}{2r^2}\left(\beta_1-\frac{1}{2}\beta_2\sin^2\theta\right) - \frac{l^2}{24r^2}\left[(\beta_1-\beta_2\cos^2\theta)-\frac{a^2}{2r^2}\left((\beta_2-\beta_3\cos^2\theta) - \tfrac{1}{2}\sin^2\theta(\beta_3-\beta_4\cos^2\theta)\right)\right]\right\} \\ &\quad + \frac{v_2}{12}l^3 z\frac{e^{ik_b r}}{r^3}\left[\beta_1-\frac{a^2}{2r^2}\left(\beta_2-\frac{1}{2}\beta_3\sin^2\theta\right)\right] + O(l^4, a^3) \end{aligned} \tag{29}$$

in which $r^2 = \rho^2 + z^2$, $\sin\theta = \rho/r$, $\cos\theta = z/r$ and

$$\begin{aligned} \beta_1 &= 1 - ik_b r \\ \beta_2 &= 3 - i3k_b r - k_b^2 r^2 \\ \beta_3 &= 15 - i15k_b r - 6k_b^2 r^2 + ik_b^3 r^3 \\ \beta_4 &= 105 - i105k_b r - 45k_b^2 r^2 + i10k_b^3 r^3 + k_b^4 r^4. \end{aligned}$$

We remark that the Taylor expansion of $p_1(a)$ will be divergent as $a \to r_0$ since the nth derivative $p_1^{(n)}(0) = o(a^{-n})$ when $z = z'$ and $\rho = a$. Hence, the above equation cannot be used to evaluate the self term and adjacent mutual term of the impedance matrix.

In the global coordinate system, the segment j is shown in Fig. 3(b). In this system, $K(x, y, z)$, r, l, z, and θ in (29) are replaced by $K_j(x, y, z)$, r_j, l_j, $\hat{l}_j \cdot \boldsymbol{r}_j$, and θ_j, in which

$$\begin{aligned} r_j^2 &= (x-x_j)^2 + (y-y_j)^2 + (z-z_j)^2, \\ \boldsymbol{r}_j &= \hat{x}(x-x_j) + \hat{y}(y-y_j) + \hat{z}(z-z_j). \end{aligned}$$

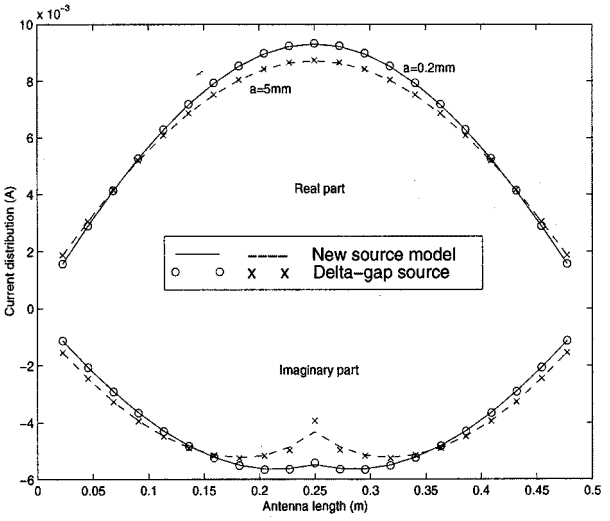

(a)

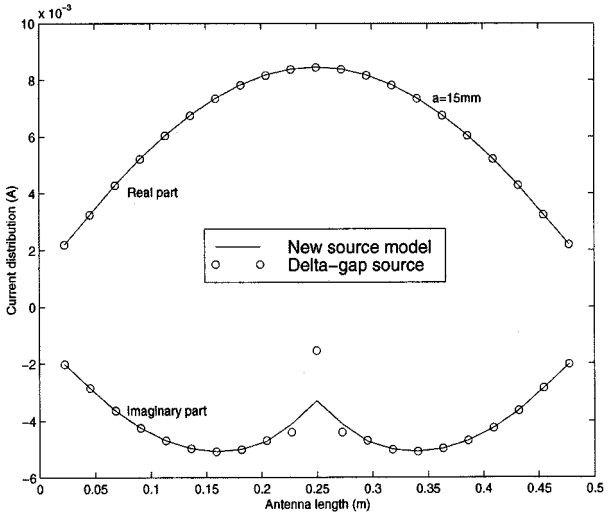

(b)

Fig. 6. Current distribution of the half-wavelength dipole with delta-gap and new source models. (a) $a = 0.2$ mm and $a = 5$ mm. (b) $a = 15$ mm.

Therefore, the mutual term

$$h(i,j) = \frac{1}{2\pi}\int_{\Delta S_i}(u_1+u_2 l)K_j(x,y,z)\,dS \tag{30}$$

is a simple integral, which can be numerically evaluated. Because the adjacent mutual term will be considered in other forms, the above equation can be approximated by

$$\begin{aligned} \phi^P(i,j) &\approx \tfrac{1}{2}l_i K_j(x_i, y_i, z_i), \\ \psi^P(i,j) &\approx l_i K_j(x_i, y_i, z_i) \end{aligned} \tag{31}$$

in which $v_1 = 1$, $v_2 = 0$ for $\psi^P(i, j)$; $v_1 = 1/2$, $v_2 = 1/l_j$ for $\phi^P(i, j)$ when $j = n_-$; $v_1 = 1/2$, $v_2 = -1/l_j$ for $\phi^P(i, j)$ when $j = n_+$.

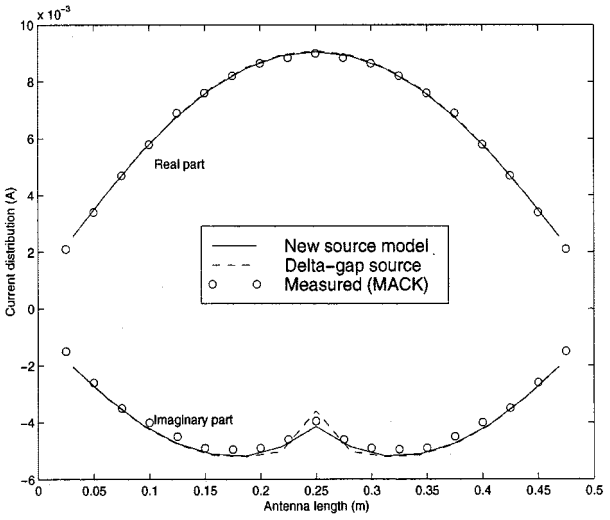

(a)

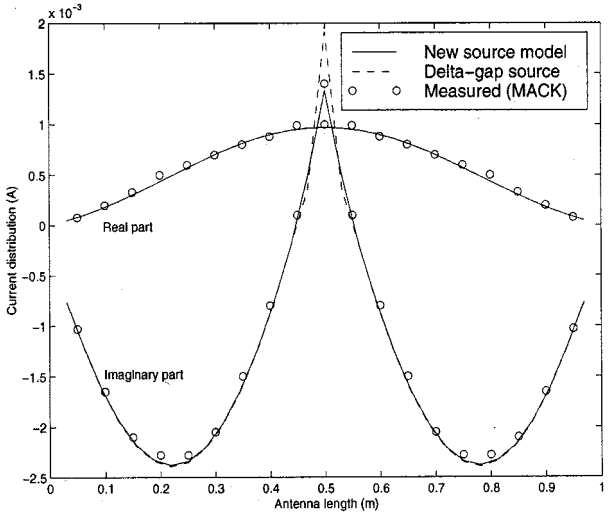

(b)

Fig. 7. Comparison of the current distributions of the new source model and delta-gap source with the measured data. (a) Half-wavelength dipole. (b) Full-wavelength dipole.

2) Self Term and Adjacent Mutual Terms: We first consider the adjacent nodes shown in Fig. 4(a), where no junction node exist. Under the local coordinate system, (27) becomes

$$h(i,j)=\frac{1}{4\pi^2}\int_0^{2\pi}d\phi\int_0^{2\pi}d\phi'\int_{z_1}^{z_2}dz(u_1+u_2z)\int_{t_1}^{t_2}\cdot dz'(v_1+v_2z')\frac{e^{ik_bR}}{R} \tag{32}$$

in which $R^2=2a^2[1-\cos(\phi-\phi')]+(z-z')^2$. Because R is electrically small for adjacent nodes, the function $p_1(R)$ can be expanded in terms of R by using Taylor's series. After a complicated derivation, we obtain a compact form for $h(i,j)$

$$\begin{aligned}h(i,j)=&-W_1+4a^2W_2+a^4W_3+2aW_4+8a^3W_5\\&+a^5W_6+i\tfrac{1}{6}k_b^3W_7+W_8+O(R^4)\end{aligned} \tag{33}$$

in which for $n=1,2,\cdots,7$

$$\begin{aligned}W_n=&F_n(t_2,z_2-t_2)\mathcal{I}_n\left(\frac{z_2-t_2}{2a}\right)\\&-F_n(t_2,z_1-t_2)\mathcal{I}_n\left(\frac{z_1-t_2}{2a}\right)\\&-F_n(t_1,z_2-t_1)\mathcal{I}_n\left(\frac{z_2-t_1}{2a}\right)\\&+F_n(t_1,z_1-t_1)\mathcal{I}_n\left(\frac{z_1-t_1}{2a}\right)\\W_8=&ik_b(z_2-z_1)(t_2-t_1)\left[u_1+\tfrac{1}{2}u_2(z_2+z_1)\right]\\&\cdot\left[v_1+\tfrac{1}{2}v_2(t_2+t_1)\right]\end{aligned}$$

where a is the radius of the wire, $\mathcal{I}_7(k)=1$ and

$$\begin{aligned}F_1(t,z)=&a_0(t)z+\tfrac{1}{2}a_1(t)z^2+\tfrac{1}{3}a_2z^3\\F_2(t,z)=&\tfrac{1}{4}k_b^2F_1(t,z)-\tfrac{1}{4}a_3\\F_3(t,z)=&\tfrac{1}{2}k_b^2a_3,\quad F_6(t,z)=-\tfrac{16}{45}k_b^2a_2\\F_4(t,z)=&a_0(t)+\tfrac{1}{4}b_2(t)z+\tfrac{1}{36}[3k_b^2a_0(t)+16a_2]z^2\\&+\tfrac{1}{48}k_b^2b_1(t)z^3+\tfrac{1}{60}k_b^2a_2z^4\\F_5(t,z)=&-\tfrac{1}{18}[3k_b^2a_0(t)-2a_2]-\tfrac{1}{96}k_b^2b_3(t)z-\tfrac{7}{90}k_b^2a_2z^2\\F_7(t,z)=&a^2z^2\left[a_0(t)+\tfrac{1}{3}a_4(t)z+\tfrac{1}{4}a_2z^2\right]\\&+\tfrac{1}{12}z^4\left[a_0(t)+\tfrac{1}{5}a_5(t)z+\tfrac{1}{6}a_2z^2\right]\end{aligned}$$

in which

$$\begin{aligned}a_0(t)=&(u_1+u_2t)(v_1+v_2t)\\a_1(t)=&u_1v_2+u_2v_1+2u_2v_2t\\a_2=&u_2v_2,\\a_3=&u_2v_1-u_1v_2\\a_4(t)=&u_1v_2+2u_2v_1+3u_2v_2t\\a_5(t)=&u_1v_2+4u_2v_1+5u_2v_2t\\b_0(t)=&u_1v_2+u_2v_2t\\b_1(t)=&u_1v_2+3u_2v_1+4u_2v_2t\\b_2(t)=&3u_1v_2+u_2v_1+4u_2v_2t\\b_3(t)=&13u_1v_2+3u_2v_1+16u_2v_2t\end{aligned}$$

and $\mathcal{I}_n(k)$ $(n=1,2,\cdots,6)$ are integrals defined as

$$\begin{aligned}\mathcal{I}_1(k)=&\frac{2}{\pi}\int_0^{\pi/2}\sinh^{-1}\frac{k}{\sin\phi}\,d\phi\\\mathcal{I}_2(k)=&\frac{2}{\pi}\int_0^{\pi/2}\sin^2\phi\,\sinh^{-1}\frac{k}{\sin\phi}\,d\phi\\\mathcal{I}_3(k)=&\frac{2}{\pi}\int_0^{\pi/2}\sin^4\phi\,\sinh^{-1}\frac{k}{\sin\phi}\,d\phi\end{aligned}$$

$$\mathcal{I}_4(k) = \frac{2}{\pi}\int_0^{\pi/2} \sqrt{k^2+\sin^2\phi}\, d\phi$$
$$\mathcal{I}_5(k) = \frac{2}{\pi}\int_0^{\pi/2} \sin^2\phi \sqrt{k^2+\sin^2\phi}\, d\phi$$
$$\mathcal{I}_6(k) = \frac{2}{\pi}\int_0^{\pi/2} \sin^4\phi \sqrt{k^2+\sin^2\phi}\, d\phi.$$

In the above integrals, the first three are odd function of k and the last three are elliptical integrals, all of which can be rapidly computed. When $k = 0$,

$$\mathcal{I}_1(0) = \mathcal{I}_2(0) = \mathcal{I}_3(0) = 0$$
$$\mathcal{I}_4(0) = \frac{2}{\pi}, \quad \mathcal{I}_5(0) = \frac{4}{3\pi}, \quad \mathcal{I}_6(0) = \frac{16}{15\pi}.$$

If all the segments have the same length, these integrals are fixed.

The self term and adjacent mutual terms can be obtained from (33) by choosing different parameters u_1, u_2, v_1, v_2, z_1, z_2, t_1, and t_2. Table I gives these parameters of adjacent nodes in which u_1, u_2, v_1, and v_2 are only for $\phi^P(i, j)$. For $\psi^P(i, j)$, they are constant: $u_1 = v_1 = 1$, $u_2 = v_2 = 0$.

If the node n is a junction point of two bend wires shown in Fig. 4(b), the formula (33) will be invalid for $h(n_+, n_-)$, $h[n_+, (n-1)_+]$, $h(n_-, n_+)$, $h[n_-, (n+1)_-]$, as well as $h[(n+1)_-, (n-1)_+]$ and $h[(n-1)_+, (n+1)_-]$. Under the local coordinate systems (x, y, z) and (x', y', z') in which x and x' are assumed to be in the same direction, (32) still holds, however, the distance R has been changed. By rotating one of the coordinate systems one easily obtains

$$R^2 = a^2(\cos\phi - \cos\phi')^2 + (a\sin\phi - a\sin\phi'\cos\theta_0 + z'\sin\theta_0)^2 + (z - a\sin\phi'\sin\theta_0 - z'\cos\theta_0)^2$$

where θ_0 is the angle between the two bend wires. Unfortunately, for this general formula we cannot obtain a closed form like (33). Using Taylor's expansion, the four-dimensional integral (32) can reduce to several three-dimensional integrals, which have to be evaluated by numerical integration.

Generally, the number of junction nodes, N_j, is very small in wire antennas. For example, $N_j = 0$ for dipoles and circular loops; $N_j = 3$ for triangle loops; and $N_j = 4$ for square loops. Therefore, no more computational burden has increased.

B. Voltage Vector

Like the electric-field dyadic Green's function shown in (3), the magnetic-field dyadic Green's function $\overline{\boldsymbol{G}}_m$ in the voltage vector (12) also contains a primary-field term and reflected-field terms. Similar to the impedance matrix, we approximate the integral $\int d\phi'$ by 2π in the reflected-field terms. Then it is easily shown that the voltage vector contributed by these terms equals zero.

Now we evaluate the contribution from the primary-field term. It is known that in an unbounded homogeneous region [27]

$$\nabla \times \overline{\boldsymbol{G}}_m(\boldsymbol{r}', \boldsymbol{r}) = \frac{1}{4\pi}\nabla \times \overline{\boldsymbol{I}} g^P(\boldsymbol{r}' - \boldsymbol{r}).$$

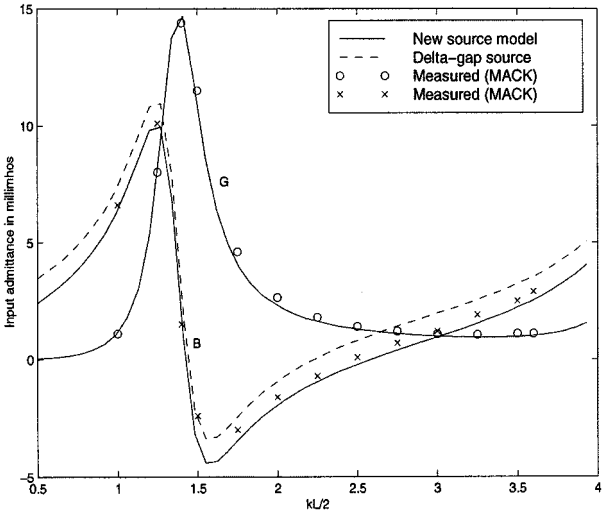

Fig. 8. Comparison of the input admittance of the two source models with the measured data.

Hence, the voltage vector becomes

$$V_n = -\frac{1}{4\pi}\langle \boldsymbol{J}_n(\boldsymbol{r}), \nabla \times \overline{\boldsymbol{I}} g^P(\boldsymbol{r} - \boldsymbol{r}'), \boldsymbol{M}_a(\boldsymbol{r}')\rangle$$
$$= -\langle \boldsymbol{J}_n(\boldsymbol{r}), \nabla \times \boldsymbol{F}_e(\boldsymbol{r})\rangle$$
$$= \langle \boldsymbol{J}_n(\boldsymbol{r}), \boldsymbol{E}_a(\boldsymbol{r})\rangle \tag{34}$$

where $\epsilon_0\tilde{\epsilon}_b\boldsymbol{F}_e$ is the electric vector potential. In the following subsections, we assume that the driving point is not a junction of two bent wires. If it is, we can use a method similar to Fig. 4(b) to compute the numerical integration.

1) Nodes Far From the Gap: The local coordinate system of the gap is shown in Fig. 3(a) in which l is replaced by Δ. In this system, $\boldsymbol{M}_a(\boldsymbol{r}') = \hat{\phi}' M_a$. Expanding the integrand in terms of the radius a and integrating around ϕ', we clearly see that $\boldsymbol{F}_e$ has only ϕ component. Expanding the resulting functions in terms of z', we obtain

$$F_{e\phi}(\boldsymbol{r}) \approx \frac{M_a}{4} a^2\Delta \sin\theta \frac{e^{ik_b r}}{r^2}(1 - ik_b r) \cdot \left\{1 + \frac{\Delta^2}{24r^2}\left[ik_b r - 2 + \cos^2\theta(8 - i5k_b r - k_b^2 r^2)\right] + \frac{\Delta^2}{24r^2(1 - ik_b r)}\left[\cos^2\theta(7 - i2k_b r) - 1\right]\right\} + O(a^3, \Delta^3). \tag{35}$$

Hence,

$$E_{a\rho} \approx -\frac{M_a}{4} a^2\Delta \sin\theta\cos\theta \frac{e^{ik_b r}}{r^3} \cdot \left(\beta_2 - \frac{\Delta^2}{8r^2}\beta_3 + \frac{\Delta^2}{24r^2}\beta_4\cos^2\theta\right) + O(a^3, \Delta^3) \tag{36}$$

$$E_{az} \approx \frac{M_a}{4} a^2\Delta \frac{e^{ik_b r}}{r^3}\left[\left(\beta_5 - \frac{\Delta^2}{24r^2}(\beta_6 - \beta_7\cos^2\theta)\right) - \cos^2\theta\left(\beta_2 - \frac{\Delta^2}{8r^2}\beta_3 + \frac{\Delta^2}{24r^2}\beta_4\cos^2\theta\right)\right] + O(a^3, \Delta^3) \tag{37}$$

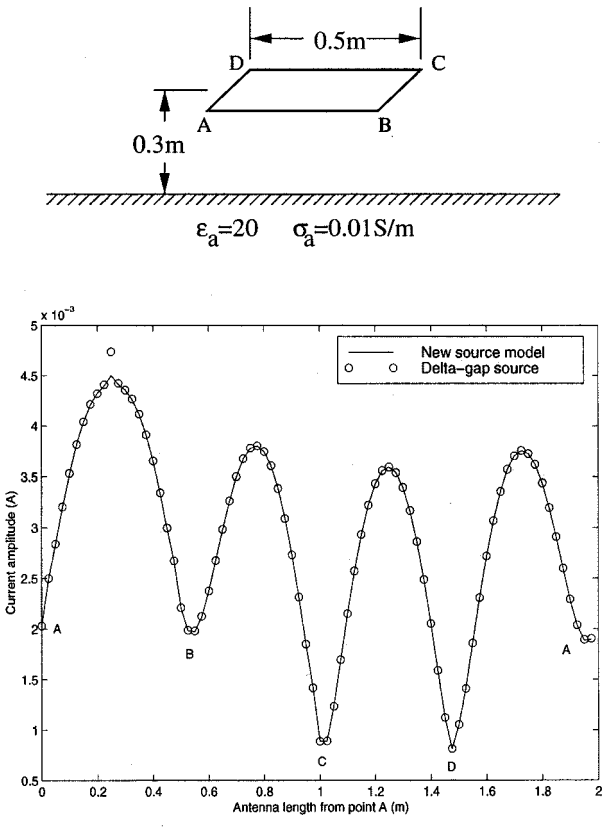

Fig. 9. Current distribution of a square loop above a clay when $f = 300$ MHz and $a = 10$ mm.

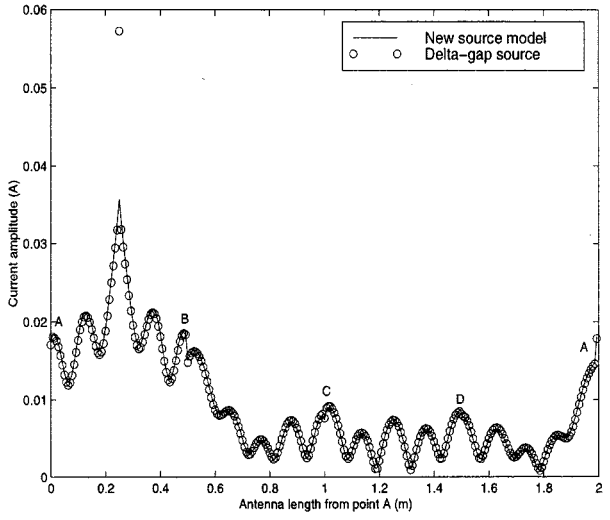

Fig. 10. Current distribution of the square loop inside the clay when $f = 300$ MHz and $a = 10$ mm.

in which

$$\beta_5 = 1 - ik_b r - k_b^2 r^2$$
$$\beta_6 = 9 - i9k_b r - 4k_b^2 r^2 + ik_b^3 r^3$$
$$\beta_7 = 45 - i45k_b r - 21k_b^2 r^2 + i6k_b^3 r^3 + k_b^4 r^4.$$

Note that (35)–(37) are invalid when $\rho = a$ and $z = z'$ due to the same reason as that in the impedance matrix. In the global coordinate system shown in Fig. 3(b), where the center coordinate, the unit tangential vector, and the unit normal vector of the gap are assumed to be (x_g, y_g, z_g), $\hat{l}_g$, and $\hat{n}_g$, respectively. Then, r, z, $\hat{\rho}$, $\hat{z}$, and θ in (35)–(37) should be replaced by r_g, $\hat{l}_g \cdot \boldsymbol{r}_g$, $\hat{n}_g$, $\hat{l}_g$, and θ_g, in which

$$r_g^2 = (x - x_g)^2 + (y - y_g)^2 + (z - z_g)^2$$
$$\boldsymbol{r}_g = \hat{x}(x - x_g) + \hat{y}(y - y_g) + \hat{z}(z - z_g).$$

Therefore, the voltage vector becomes

$$V_n = \frac{1}{2\pi}\int_0^{2\pi} d\phi \int_{-l_{n_-}}^{0} dl(1 + l/l_{n_-}) \cdot \left[\hat{l}_{n_-} \cdot \hat{n}_g E_{a\rho}(x, y, z) + \hat{l}_{n_-} \cdot \hat{l}_g E_{az}(x, y, z)\right] + \frac{1}{2\pi}\int_0^{2\pi} d\phi \int_0^{l_{n_+}} dl(1 - l/l_{n_+}) \cdot \left[\hat{l}_{n_+} \cdot \hat{n}_g E_{a\rho}(x, y, z) + \hat{l}_{n_+} \cdot \hat{l}_g E_{az}(x, y, z)\right]. \quad (38)$$

Because the nodes adjacent to the gap will be considered in other forms, (38) can be further approximated by

$$V_n \approx \tfrac{1}{2} l_{n_-} \left[\hat{l}_{n_-} \cdot \hat{n}_g E_{a\rho}(x_{n_-}, y_{n_-}, z_{n_-}) + \hat{l}_{n_-} \cdot \hat{l}_g E_{az}(x_{n_-}, y_{n_-}, z_{n_-})\right] + \tfrac{1}{2} l_{n_+} \left[\hat{l}_{n_+} \cdot \hat{n}_g E_{a\rho}(x_{n_+}, y_{n_+}, z_{n_+}) + \hat{l}_{n_+} \cdot \hat{l}_g E_{az}(x_{n_+}, y_{n_+}, z_{n_+})\right]. \quad (39)$$

2) Nodes Adjacent to the Gap: Under the local coordinate system shown in Fig. 4(a), the voltage vector (34) can be written as the following general form for adjacent nodes:

$$V(z_1, z_2, u_1, u_2) = \frac{M_a}{8\pi^2} a^2 \int_0^{2\pi} d\phi \int_0^{2\pi} d\phi' [1 - \cos(\phi - \phi')] \cdot \int_{z_1}^{z_2} dz(u_1 + u_2 z) \int_{-\Delta/2}^{\Delta/2} dz' \frac{ik_b R - 1}{R^3} e^{ik_b R} \quad (40)$$

in which $R^2 = 2a^2[1 - \cos(\phi - \phi')] + (z - z')^2$. Expanding the integrand in terms of R by using Taylor's series, we obtain a compact form for $V(z_1, z_2, u_1, u_2)$

$$V(z_1, z_2, u_1, u_2) \approx -M_a a(U_2 + U_3 + U_4 + U_5 + U_8) + O(R^4) \quad (41)$$

in which for $n = 2, 3, 4, 5$

$$U_n = D_n\left(-\Delta, z_2 + \frac{\Delta}{2}\right)\mathcal{I}_n\left(\frac{2z_2 + \Delta}{4a}\right) - D_n\left(-\Delta, z_1 + \frac{\Delta}{2}\right)\mathcal{I}_n\left(\frac{2z_1 + \Delta}{4a}\right) - D_n\left(\Delta, z_2 - \frac{\Delta}{2}\right)\mathcal{I}_n\left(\frac{2z_2 - \Delta}{4a}\right) + D_n\left(\Delta, z_1 - \frac{\Delta}{2}\right)\mathcal{I}_n\left(\frac{2z_1 - \Delta}{4a}\right)$$
$$U_8 = i\tfrac{1}{6} k_b^3 a\Delta(z_2 - z_1)\left[u_1 + \tfrac{1}{2} u_2(z_2 + z_1)\right]$$

where $\mathcal{I}_2(k)$ to $\mathcal{I}_5(k)$ are integrals defined as before and

$$D_2(t, z) = -\tfrac{1}{2} u_2 a + \tfrac{1}{4} k_b^2 az[2u_1 + u_2(z + t)]$$
$$D_3(t, z) = \tfrac{1}{2} u_2 k_b^2 a^3$$
$$D_4(t, z) = \tfrac{1}{4}[2u_1 + u_2(z + t)]$$
$$D_5(t, z) = -\tfrac{1}{4} k_b^2 a^2[4u_1 + u_2(z + 2t)].$$

Then the voltage vector for the adjacent nodes are given by

$$V_g = V\left(-l_{g_-}, 0, 1, l_{g_-}^{-1}\right) + V\left(0, l_{g_+}, 1, -l_{g_+}^{-1}\right) \quad (42)$$

$$V_{g-1} = V\left(-l_{g_-}, 0, 0, -l_{g_-}^{-1}\right) + V\left(-l_{g_-} - l_{(g-1)_-}, -l_{g_-}, 1 + l_{g_-} l_{(g-1)_-}^{-1}, l_{(g-1)_-}^{-1}\right) \quad (43)$$

$$V_{g+1} = V\left(0, l_{g_+}, 0, l_{g_+}^{-1}\right) + V\left(l_{g_+}, l_{g_+} + l_{(g+1)_+}, 1 + l_{g_+} l_{(g+1)_+}^{-1}, -l_{(g+1)_+}^{-1}\right). \quad (44)$$

Similar expressions can be found for V_{g-2} and V_{g+2}.

IV. Numerical Results

To test the validity of the accurate model, we consider a simple example: a dipole in free space so that the numerical results can be compared with measured data.

As stated in the previous sections, the impedance matrix, the source model and the definition of input admittance have been improved in the accurate model. So, we first see the modification of the impedance matrix. Table II shows the comparison of impedance matrices of half-wavelength dipole computed by the accurate model and the old model [26] when the wire radius changes from 0.2 to 15 mm, in which, $f = 300$ MHz and 21 nodes have been used. In the old model, the electric current is assumed to flow on the axis of the wire.

From Table II, the impedance matrix computed by the accurate model is nearly the same as that by the old model when the wire is very thin. This is because the current is nearly concentrated on the axis in this case. When the wire radius increases, the difference between the two models increases. Fig. 5 gives the comparison of current distribution of the three radius in which the delta-gap source model has been used. As expected, the current distributions by the two models are nearly the same when the wire is very thin. However, they are also very close when $a = 5$ mm although the impedance matrix changes a lot. When the wire radius increases to 15 mm, the old model is invalid, as shown in Fig. 5(b).

Next, we observe the voltage vector of the new source model. Table III illustrates the comparison of source vectors of the same dipole for different wire radius, in which the driving voltage is set to 1 V. To save space, only half of the vector is given which is symmetrical. From Table III, two interesting phenomena can be observed: 1) the source vector approaches to the delta function when the wire radius is very thin; as the radius increases, the sharp delta function becomes broader and 2) the summation of the source-vector elements is a constant which just equals the driving voltage.

To compare the delta-gap and new source models, Fig. 6 shows the current distributions along the dipole in which and later examples, the impedance matrix is computed by the accurate model. We clearly see that the electric current near the driving point has a larger difference in the two models when the wire radius increases, which directly affects the accuracy of the input admittance.

To test the validity of the accurate model, a comparison of current distributions by the numerical results and measured data is plotted in Fig. 7 in which $f = 300$ MHz, $a = 7.022$ mm, and 15 and 31 nodes have been used for half-wavelength and full-wavelength dipoles. The measured data are obtained from [9] and [10]. From Fig. 7, the current distribution from the new model is much closer to the measured data than that of the delta-gap model, especially for the full-wavelength dipole. Therefore, the input admittance of this model is also more accurate. Fig. 8 shows the comparison of the input admittance of the two models and measured data [9], [11] in which $a = 0.007\,002\lambda$. Clearly, the new model is much closer to the measured data.

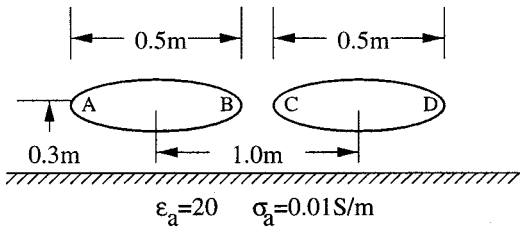

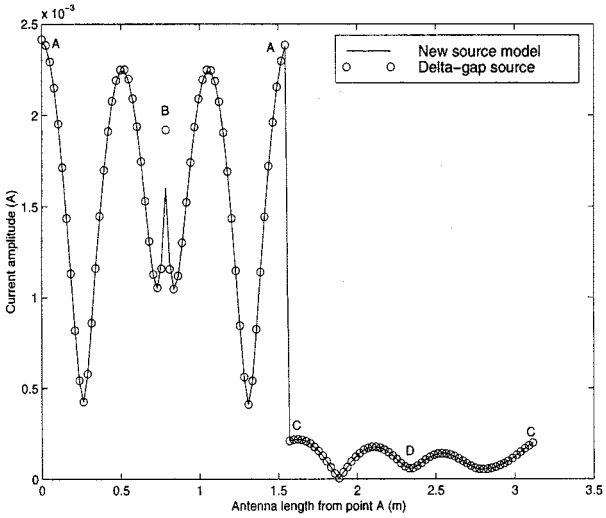

Fig. 11. Current distribution of two circular loops above the clay when $f = 300$ MHz and $a = 5$ mm.

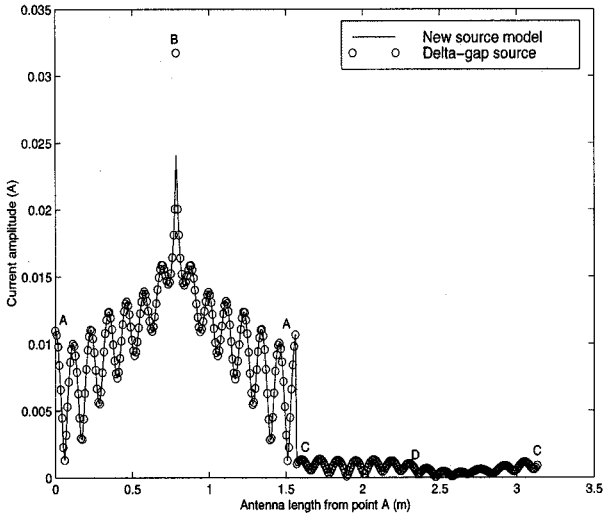

Fig. 12. Current distribution of two circular loops inside the clay when $f = 300$ MHz and $a = 5$ mm.

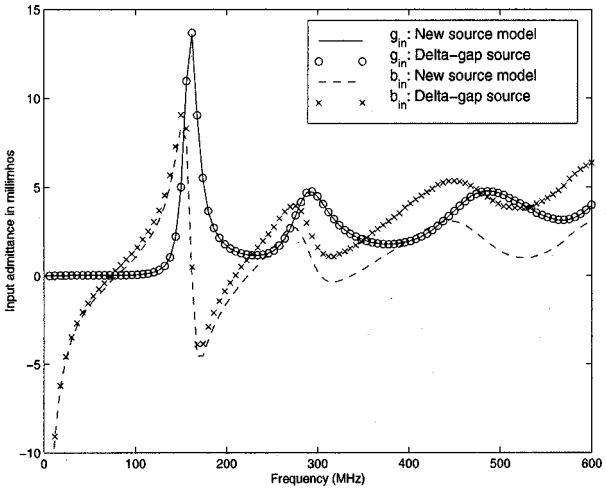

(a)

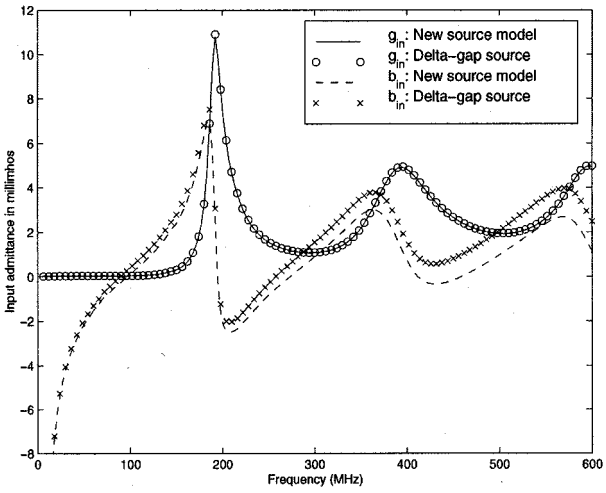

(b)

Fig. 13. Input admittance of the square and circular loops above the clay. (a) Square loop. (b) Circular loops.

Now we consider some complicated wire shapes. When a square loop is placed 0.3 m above a clay ($\epsilon_a = 20$ and $\sigma_a = 0.01$ S/m), the current distributions computed by the two models are illustrated in Fig. 9 in which the feed point is located at the center of line **AB** and 80 segments have been used. When the same loop is placed 0.3 m under the clay, the current distributions are displayed in Fig. 10. In this case, however, 280 segments have been chosen since the electric size of the loop increases.

Fig. 11 illustrates the current distribution of two circular loops above the clay, in which the feed point is driven at the center of arc **AB** and 120 segments have been used. When the same circular loops are set 0.3 m under the clay, the current distribution is depicted in Fig. 12, where the loops are discretized into 360 segments.

From Figs. 9–12, the current distributions computed by the two source models are nearly the same, except near the feed point, which directly affect the input admittance. The comparison of input admittance of the loops above the clay computed by the delta-gap and new source models are shown in Fig. 13 when the frequency changes from 0 to 600 MHz. From this figure, we notice that the real parts computed by the two models are nearly identical but the imaginary parts are quite different, especially in high frequency.

V. Conclusions

This paper presents an accurate model for arbitrary wire antennas in the free space, above or inside the lossy ground by using the Galerkin's method. Comparing with old models, three improvements have been made.

- The current is assumed to flow on the surface of the wire and the testing is also performed on the surface. Numerical results show that only when the wire is very thin can the current be considered to flow on the axis.
- A new source model has been presented to replace the delta gap. Numerical results show that only when the wire is very thin, does the source vector approach to the delta function (delta gap).
- A variational formula of the input admittance has been obtained. In fact, this is a general formula. The traditional definition is only a special case of this formula when the source vector is a delta function.

Although the new model provides more accurate results, its numerical complexity and storage requirements keep the same compared with the old models. They have the same convergence rate as the number of segments is increased.

Acknowledgment

This paper is dedicated to the memory of M. P. Ekstrom, an avid supporter of geo-electromagnetics and an upholder of principles and integrity.

References

[1] H. C. Pocklington, "Electrical oscillations in wire," *Cambridge Philos. Soc. Proc.*, vol. 9, pp. 324–332, 1897.
[2] A. Sommerfeld, "Uber die ausbreitung der wellen in der drahtlosen telegraphie," *Annalen der Physik (4th Folge)*, vol. 28, pp. 665–736, 1909.
[3] E. Hallen, "Theoretical investigations into the transmitting and receiving qualities of antennae," in *Nova Acta Regiae Soc. Sci. Upsaliensis*, ser. IV, 1938, pp. 1–44.
[4] R. W. P. King and C. W. Harrison Jr., "The distribution of current along a symmetric center-driven antenna," *Proc. IRE*, vol. 31, pp. 548–567, Oct. 1943.
[5] C. T. Tai, "A new interpretation of the integral equation formulation of cylindrical antennas," *IRE Trans. Antennas Propagat.*, vol. AP-3, pp. 125–127, Feb. 1955.
[6] J. H. Richmond, "A wire-grid model for scattering by conducting bodies," *IEEE Trans. Antennas Propagat.*, vol. AP-14, pp. 782–786, Nov. 1966.
[7] R. F. Harrington, *Field Computation by Moment Methods*. New York: McMillan, 1968.
[8] C. M. Butler and D. R. Wilton, "Analysis of various numerical techniques applied to thin-wire scatterers," *IEEE Trans. Antennas Propagat.*, vol. AP-23, pp. 534–540, 1975.
[9] R. B. Mack, "A study of circular arrays," Harvard University, Cruft Lab. Tech. Rep. 381-386, May 1963.
[10] R. W. P. King, G. S. Smith, M. Owens, and T. T. Wu, *Antennas in Matter—Fundamental, Theory, and Applications*. Cambridge, MA: MIT Press, 1981, pp. 150–156.

[11] R. S. Elliott, *Antenna Theory and Design*. Englewood Cliffs, NJ: Prentice-Hall, 1981, p. 318.
[12] Y. T. Lo and S. W. Lee (Eds, *Antenna Handbook: Theory, Applications, and Design*. New York: Van Nostrand Reinhold, 1988.
[13] C. A. Balanis, *Antenna Theory: Analysis and Design*, 2nd ed. New York: Wiley, 1997.
[14] A. Banos, *Dipole Radiation in the Presence of a Conducting Half-Space*. Oxford, U.K.: Pergamon Press, 1966.
[15] D. C. Chang and J. R. Wait, "Appraisal of near-field solutions for a Hertzian dipole over a conducting half-space," *Can. J. Phys.*, vol. 48, pp. 737–743, 1970.
[16] E. K. Miller, A. J. Poggio, G. J. Burke, and E. S. Selden, "Analysis of wire antennas in the presence of a conducting half-space: Part I—The vertical antenna in free space," *Can. J. Phys.*, vol. 50, pp. 879–888, 1972.
[17] D. C. Chang and R. Fisher, "A unified theory on radiation of a vertical electric dipole above a dissipative earth," *Radio Sci.*, vol. 9, pp. 1129–1138, 1974.
[18] S. M. Ali and S. F. Mahmoud, "Electromagnetic fields of buried sources in stratified anisotropic media," *IEEE Trans. Antennas Propagat.*, vol. AP-27, pp. 671–678, Sept. 1979.
[19] L. N. An and G. S. Smith, "The horizontal circular loop antenna near a planar interface," *Radio Sci.*, vol. 17, pp. 483–502, 1982.
[20] Y. Rahmat-Samii, R. Mittra, and P. Parhami, "Evaluation of Sommerfeld integrals for lossy half-space problems," *Electromagn.*, vol. 1, pp. 1–28, 1981.
[21] G. J. Burke, A. J. Poggio, J. C. Logan, and J. W. Rockway, "NEC—Numerical electromagnetic code for antennas and scattering," in *IEEE AP-S Int. Symp. Dig.*, Seattle, WA, June 1979, pp. 147–150.
[22] G. J. Burke, E. K. Miller, J. N. Brittingham, D. L. Lager, R. J. Lytle, and J. T. Okada, "Computer modeling of antennas near the ground," *Electromagn.*, vol. 1, pp. 29–49, 1981.
[23] K. A. Michalski and J. R. Mosig, "Multilayered media Green's functions in integral equation formulations," *IEEE Trans. Antennas Propagat.*, vol. 45, pp. 508–519, Mar. 1997.
[24] J. S. Zhao, W. C. Chew, C. C. Lu, E. Michielssen, and J. M. Song, "Thin-stratified medium fast-multipole algorithm for solving microstrip structures," *IEEE Trans. Microwave Theory Tech.*, vol. 46, pp. 395–403, Apr. 1998.
[25] T. J. Cui and W. C. Chew, "Fast evaluation of Sommerfeld integrals for EM wave scattering and radiation by three-dimensional buried objects," *IEEE Trans. Geosci. Remote Sensing*, vol. 37, pp. 887–900, Mar. 1999.
[26] ——, "Modeling of arbitrary wire antennas above ground," *IEEE Trans. Geosci. Remote Sensing*, pt. 2, vol. 38, pp. 357–365, Jan. 2000.
[27] W. C. Chew, *Waves and Fields in Inhomogeneous Media*, 2nd ed. Piscataway, NJ: IEEE Press, 1995.
[28] W. C. Chew, Z. P. Nie, Q. H. Liu, and Y. T. Lo, "Analysis of a probe-fed microstrip disk antenna," *Proc. Inst. Elect. Eng.*, pt. H, vol. 138, pp. 185–191, Apr. 1991.

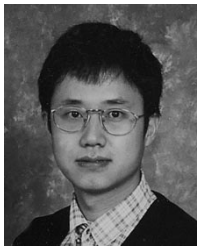

Tie Jun Cui (M'98) was born on September 8, 1965, in Hebei, China. He received the B.Sc., M.Sc., and Ph.D. degrees in electrical engineering from Xidian University, Xi'an, China, in 1987, 1990, and 1993, respectively.

In March 1993, he joined the Department of Microwave Telecommunications Engineering, Xidian University. He became an Associate Professor in November 1993 at the same university. From 1995 to 1997 he was a Research Fellow with the Institut für Höchstfrequenztechnik und Elektronik (IHE), University of Karlsruhe, Germany. In July 1997 he became a Postdoctoral Research Associate at the Center for Computational Electromagnetics, Department of Electrical and Computer Engineering, University of Illinois at Urbana-Champaign. His research interests include electromagnetic scattering and inverse scattering, wave propagation, and numerical methods. Recently, he conducted the research of fast algorithms for buried objects, the modeling of wire antennas above or inside the lossy ground, and landmine detection.

Dr. Cui received a Research Fellowship from the Alexander von Humboldt Foundation, Bonn, Germany, in 1995, and the URSI Young Scientist Award at the URSI General Assembly, Toronto, in 1999. He is a member of Commission B of URSI and senior member of the Chinese Institute of Electronics (CIE).

Weng Cho Chew (S'79–M'80–SM'86–F'93) was born on June 9, 1953, in Malaysia. He received the B.S. degree in 1976, both the M.S. and Engineer degrees in 1978, and the Ph.D. degree in 1980, all in electrical engineering, from the Massachusetts Institute of Technology, Cambridge.

From 1981 to 1985, he was with Schlumberger-Doll Research in Ridgefield, Connecticut. While he was there, he was a Program Leader and later a Department Manager. From 1985 to 1990 he was an Associate Professor with the University of Illinois. He currently is a Professor there and teaches graduate courses in waves and fields in inhomogeneous media and theory of microwave and optical waveguides. He also supervises a graduate research program. From 1989 to 1993, he was the Associate Director of the Advanced Construction Technology Center at the University of Illinois. Presently, he is the Director of the Center for Computational Electromagnetics and the Electromagnetics Laboratory at the same university. He has authored *Waves and Fields in Inhomogeneous Media* (Piscataway, NJ: IEEE Press, 1995, 2nd ed.), published over 190 scientific journal articles and presented over 200 conference papers. He is an associate editor of *Journal of Electromagnetic Waves and Applications* (1996–present), and *Microwave Optical Technology Letters* (1996–present). He was also an associate editor with the *International Journal of Imaging Systems and Technology* (1989–1994), and has been a guest editor of *Radio Science* (1986), *International Journal of Imaging Systems and Technology* (1989), and *Electromagnetics* (1995). His recent research interest has been in the area of wave propagation, scattering, inverse scattering, and fast algorithms related to scattering, inhomogeneous media for geophysical subsurface sensing and nondestructive testing applications. Previously, he also analyzed electrochemical effects and dielectric properties of composite materials, microwave and optical waveguides, and microstrip antennas.

Dr. Chew is a member of Eta Kappa Nu, Tau Beta Pi, URSI Commissions B and F, and an active member with the Society of Exploration Geophysics. He was an NSF Presidential Young Investigator for 1986. He was also an AdCom Member IEEE Geoscience and Remote Sensing Society and is presently an Associate Editor of the IEEE TRANSACTIONS OF GEOSCIENCE AND REMOTE SENSING (1984-present). His name is listed many times in the *List of Excellent Instructors* on campus.